JBC RESEARCH ARTICLE

Spermine attenuates TGF-β-induced EMT by downregulating fibronectin

Received for publication, August 22, 2024, and in revised form, January 13, 2025 Published, Papers in Press, February 25, 2025,
https://doi.org/10.1016/j.jbc.2025.108352

Huidong Liu[1] **and Ye-Guang Chen**[1,2,*]

From the [1]*The State Key Laboratory of Membrane Biology, Tsinghua-Peking Center for Life Sciences, School of Life Sciences, Tsinghua University, Beijing, China;* [2]*The MOE Basic Research and Innovation Center for the Targeted Therapeutics of Solid Tumors, School of Basic Medical Sciences, Jiangxi Medical College, Nanchang University, Nanchang, China*

Reviewed by members of the JBC Editorial Board. Edited by Donita C. Brady

Epithelial–mesenchymal transition (EMT) is a highly dynamic cellular process that occurs in development, tissue repair, and cancer metastasis. As a master EMT inducer, transforming growth factor-beta (TGF-β) can activate the EMT program by regulating the expression of key EMT-related genes and triggering other required cellular changes. However, it is unclear whether cell metabolism is involved in TGF-β-induced EMT. Here, we characterized early metabolic changes in response to transient TGF-β stimulation in HaCaT cells and discovered that TGF-β signaling significantly reduces the intracellular polyamine pool. Exogenous addition of spermine, but not other polyamines, attenuates TGF-β-induced EMT. Mechanistically, spermine downregulates the extracellular matrix protein fibronectin. Furthermore, we found that TGF-β activates extracellular signal–regulated kinase to enhance the expression of spermine oxidase, which is responsible for the reduced spermine concentration. This action of TGF-β on EMT *via* the polyamine metabolism provides new insights into the mechanisms underlying EMT and might be exploited as a way to target the EMT program for therapy.

Epithelial–mesenchymal transition (EMT), in which polarized epithelial cells acquire a highly motile mesenchymal phenotype, plays an important role in animal development, tissue regeneration, and repair as well as in disease progression including fibrosis and cancer (1–5). Cells undergoing EMT are often characterized by loss of cell–cell junctions, cytoskeletal reorganization, gene expression reprogramming, and increased cell motility, which are controlled by a variety of signaling cues (6–8). As the most well-studied pathway known to induce EMT, transforming growth factor-beta (TGF-β) signaling has been documented to activate the EMT process through multiple layers of controls, involving epigenetic, transcriptional, post-transcriptional, translational, and post-translational regulation, spanning from DNA to mRNA to protein (9–13).

Cellular metabolites, previously recognized as the most downstream and passive products of a cell's central molecular machinery (genes, mRNAs, and proteins), are later uncovered able to actively modulate the operation of this larger system and impact cell physiology in diverse contexts (14–17). Indeed, a growing body of evidence has shown that metabolic alteration is required for the occurrence or sustaining of EMT (18, 19). For instance, reduced fructose-1,6-biphosphatase expression is required for Snail-induced EMT in mammary cancer cells by conferring metabolic benefits, including augmented glycolysis and inhibited oxidative phosphorylation (20). In contrast, enhanced oxygen consumption and energy production was observed in lung cancer cells undergoing EMT, resulting from inhibited expression of fatty acid synthase (21). Besides, accumulation of fumarate elicits EMT *via* epigenetic repression of miR-200 that inhibits the expression of EMT transcription factors (22). Accumulation of dihydropyrimidine is required for EMT, possibly by acting as signaling molecules, but the explicit mechanisms need further investigation (23).

Polyamines are small positively charged molecules coupled to amino acid metabolism. Putrescine is the first product in the mammalian polyamine biosynthetic pathway, formed by the action of the first rate-limiting enzyme, ornithine decarboxylase, using ornithine as the precursor, and is successively converted by spermidine synthase and spermine synthase into higher polyamines, spermidine and spermine, respectively, which requires an aminopropyl donor provided by the second rate-limiting enzyme S-adenosylmethionine decarboxylase (Fig. 1*D*). The higher polyamines can be converted back into lower forms through a two-step reaction catalyzed by spermidine/spermine-N1-acetyltransferase and polyamine oxidase. Notably, spermine can be directly converted into spermidine by spermine oxidase (SMOX). Aside from their established roles in cell proliferation and tumorigenesis (24–26), recent studies have unveiled an extensive engagement of polyamines in an array of cellular processes, including immune regulation (27–33), inflammation (34, 35), aging (36–38), and cell survival (39, 40).

It is largely unexplored, however, whether and how TGF-β signaling could induce EMT through metabolic modulation. Several notable studies pertained to this question (41–46), yet all with prolonged TGF-β treatment and therefore cannot distinguish the changes in metabolites directly controlled by TGF-β signals or the late stages of the EMT program from secondary effects. In this study, we capitalized on untargeted

* For correspondence: Ye-Guang Chen, ygchen@tsinghua.edu.cn.

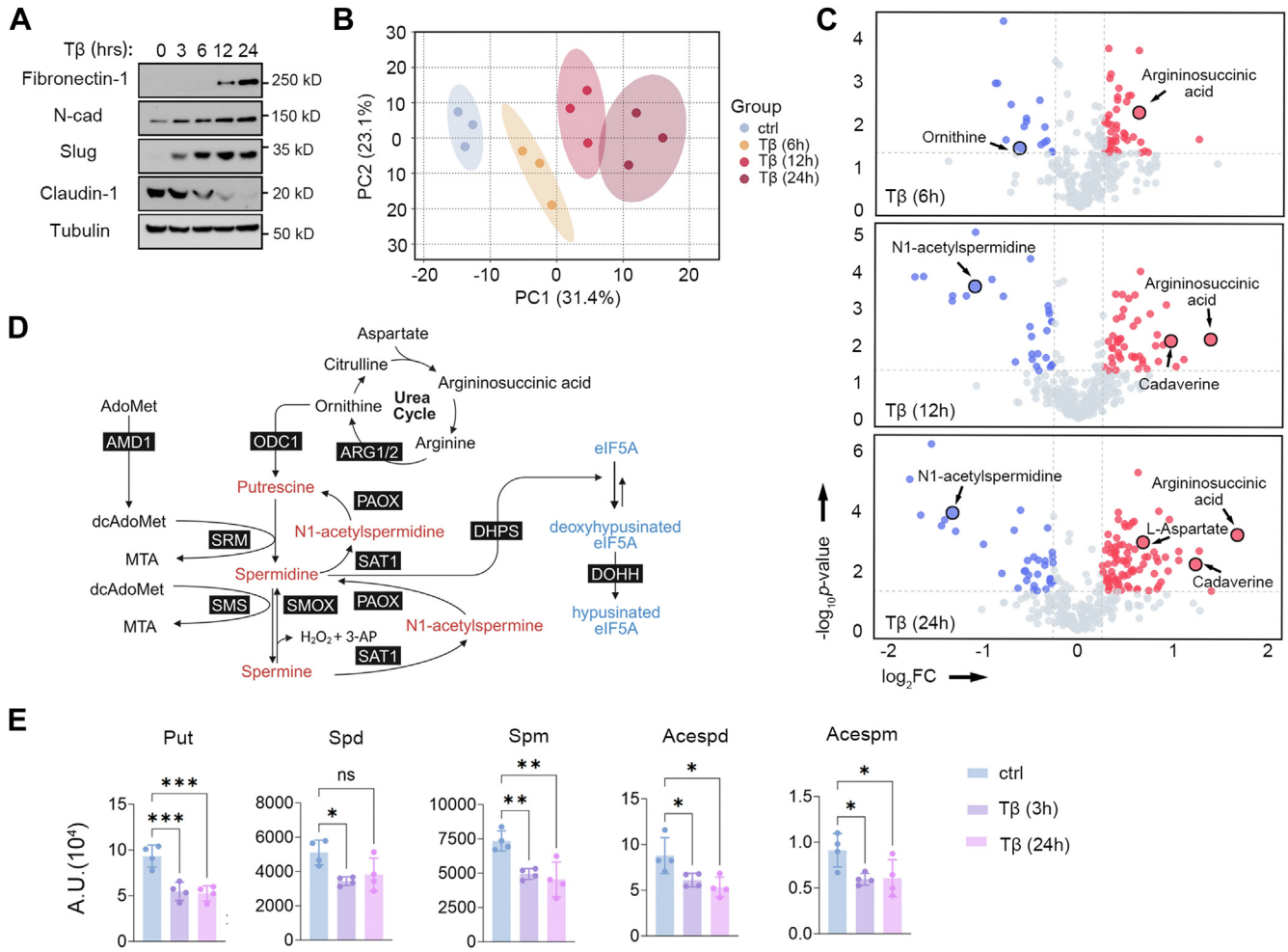

Figure 1. TGF-β reduces cellular polyamine levels in the early phase of EMT. *A*, HaCaT cells were treated with 100 pM TGF-β for the indicated times and were harvested for immunoblotting to examine the expression of EMT markers. Tubulin serves as a loading control. *B*, principal component analysis (PCA) of untargeted metabolomics. *C*, volcano plots of altered metabolites induced by TGF-β at different times. *Red and blue dots* indicate increased and decreased metabolites, respectively, with |fold change| >1.2 and $p < 0.05$ by unpaired two-tailed Student's *t* test. *D*, a schematic representation of the polyamine metabolic pathway. *E*, determination of cellular polyamine concentrations in HaCaT cells following TGF-β stimulation at the indicated times. Data are presented as mean ± SD from n = 4 biological replicates. *$p < 0.05$, **$p < 0.01$, and ***$p < 0.001$, by one-way ANOVA with Dunnett's test. AdoMet, S-adenosylmethionine; AMD1, adenosylmethionine decarboxylase 1; 3-AP, 3-aminopropanal; ARG1/2, arginase 1/2; dcAdoMet, S-adenosyl-5′-(3-methylthiopropylamine); DHPS, deoxyhypusine synthase; DOHH, deoxyhypusine hydroxylase; MTA, 5′-methylthioadenosine; ODC1, ornithine decarboxylase 1; PAOX, polyamine oxidase; SAT1, spermidine/spermine-N1-acetyltransferase; SMOX, spermine oxidase; SMS, spermine synthase; SRM, spermidine synthase; TGF-β, transforming growth factor-beta.

metabolomics analysis to specifically characterize the TGF-β early responsive metabolic reprogramming that accompanies EMT. This led us to discover reduced cellular polyamine levels by TGF-β in the early EMT phases, and in particular, spermine could significantly attenuate the TGF-β-induced EMT program, partly by downregulating the level of fibronectin-1 (FN-1).

Results

TGF-β decreases intracellular polyamine levels in the early stages of EMT

To capture the early metabolic responses induced by TGF-β signaling that may be involved in EMT, we treated cells with a low dosage of TGF-β (100 pM) over various time courses. The spontaneously immortalized HaCaT human keratinocytes were used (47), which are well responsive to TGF-β-induced EMT and nontumorigenic and should be relatively spared from metabolic changes arising secondary to neoplastic transformation.

We first confirmed a progressive EMT program as the exposure time of cells to TGF-β increased, noting that cells with a polygonal epithelial structure gradually displayed a spindle-like morphology (Fig. S1*A*). Consistently, the expression of mesenchymal markers, FN-1, N-cadherin, and Slug, was upregulated, whereas the expression of the epithelial marker claudin-1 was downregulated in a time-dependent manner (Fig. 1*A*). Based on the observation that changes in the expression of most EMT markers were manifested after 6 h of TGF-β treatment and the EMT phenotype was pronounced at 24 h, we investigated the metabolic reprogramming of HaCaT cells at 6, 12, and 24 h by untargeted metabolomics.

Principal component analysis revealed an increasingly differential pattern of metabolic profiles over the time courses of TGF-β treatment (Fig. 1*B*). Among all the metabolites detected, the levels of ornithine, argininosuccinic acid, N^1-acetylspermidine, cadaverine, and L-aspartate, were significantly changed and among the top altered metabolites (Figs. 1*C* and S1*B*). Pathway analysis further corroborated that aspartate metabolism as well as arginine and proline metabolism were among the top impacted pathways, whereas ammonia recycling, urea cycle, and spermidine and spermine biosynthesis were also affected at certain time points (Fig. S1*C*).

The five top altered metabolites and the significantly impacted metabolic pathways are closely related to polyamine metabolism (Fig. 1*D*), which prompted us to investigate whether TGF-β signaling could directly modulate the polyamine pathway. To this end, we conducted a targeted analysis of polyamine levels. Indeed, the levels of all intracellular polyamines or their acetyl derivatives were significantly reduced as early as 3 h TGF-β stimulation (Fig. 1*E*). Furthermore, the concentration of secreted polyamines in the medium also showed a decreasing trend at 3 h (residual polyamines in Dulbecco's modified Eagle's medium [DMEM] containing 0.2% fetal bovine serum [FBS] were negligible), albeit statistically insignificant (Fig. S1*D*). Taken together, our findings show that TGF-β directly regulates polyamine metabolism and diminish intracellular polyamine levels in the early stages of EMT.

Spermine counteracts the TGF-β-induced EMT program

We next asked whether the reduced polyamine levels might play a role in TGF-β-induced EMT. Hypusination of the translation elongation factor eIF5A, which requires spermidine, activates eIF5A activity to allow effective translation of proteins containing specific amino acid motifs (48–50). However, we did not observe an increased level of hypusinated eIF5A during TGF-β-induced EMT in both HaCaT and MCF10A cells (Fig. S2, *A*–*D*). Inhibition of hypusination by the small molecule GC-7 had no effect on the expression of most EMT markers at the protein level except Snail in MCF10A cells (Fig. S2, *A* and *C*). Therefore, the polyamine–eIF5A axis was unlikely to mediate the EMT program induced by TGF-β.

We then treated HaCaT cells with individual polyamines or polyamine-related metabolites to see whether these polyamine molecules may directly influence the EMT process. Among all the tested metabolites, only spermine showed the most pronounced attenuation on the expression of EMT markers (Figs. 2*A* and S2*E*), and this effect appeared to be dosage dependent (Figs. 2*B* and S2*F*). Spermine addition also restricted the spreading morphology, rescued membranous E-cadherin expression, reduced FN-1 deposition, and impeded the formation of F-actin stress fibers (Fig. 2, *C* and *D*). In addition, the enhanced migration by TGF-β was significantly compromised in cells with spermine treatment (Fig. 2*E*). To determine whether the spermine effects are cell type specific, we also examined the role of spermine in EMT using the nontransformed human mammary epithelial MCF10A cell line. In agreement with the results from HaCaT cells, spermine administration suppressed the typical morphological changes as well as the elevated expression of mesenchymal markers during EMT in MCF10A cells (Fig. 2, *F*–*H*). These results collectively indicate that spermine interferes with the TGF-β-induced EMT process.

Spermine reduces FN-1 fibrils without inhibiting the protein synthesis

We then explored the mechanism underlying spermine attenuation of TGF-β-induced EMT. We first excluded the possibility of cellular toxicity of spermine, as cell proliferation remained unchanged in the spermine-treated groups (Fig. S3*A*). The activity of the TGF-β-sensitive CAGA-luciferase reporter was also minimally affected by spermine (Fig. S3*B*), indicating spermine did not mainly impact the TGF-β signaling pathway, and its effects might be more specific to the EMT program. Since polyamines have been proposed to be capable of controlling gene expression (51, 52), we examined the expression of EMT markers at the transcriptional level. Unexpectedly, we observed inconsistency in the expression of the mesenchymal markers at the mRNA and protein levels across parallel experiments, in which the gene expression of *FN1* and *SNAI2* remained unchanged while their protein products showed a significant reduction (Fig. 3, *A*–*C*). These data suggest that spermine influences the protein levels of EMT markers.

Although serving as a well-known marker of EMT induced by TGF-β, FN-1 has been also reported to stimulate EMT in mammary epithelial cells (53). Thus, we wondered whether the decreased FN-1 level induced by spermine might contribute to the attenuation of EMT. Since FN-1 is a secreted protein that functions in the form of a fibrillar matrix (54), we first performed deoxycholic acid (DOC) extraction to examine whether spermine influences the functional extracellular matrix (ECM) FN-1. Indeed, spermine treatment decreased both the DOC-soluble (intracellular) and DOC-insoluble (ECM) fraction (Fig. 3*D*). To delve further into the mechanisms, we leveraged the O-propargyl-puromycin (OPP) labeling of nascent proteins to investigate whether spermine retards FN-1 synthesis (Fig. 3*E*). Interestingly, the abundance of newly synthesized FN-1 appeared to be slightly increased by spermine in cells undergoing TGF-β-induced EMT (Fig. 3*F*). In tandem with the observation that the concentration of secreted FN-1 remained virtually constant regardless of spermine treatment (Fig. 3*D*), this implies that spermine might downregulate FN-1 fibrils by influencing their assembly or degradation.

Fibronectin coating accelerates EMT and partially rescues spermine effects

We then addressed whether the FN-1 matrix can potentiate EMT response. After plating HaCaT cells on Matrigel- or FN-

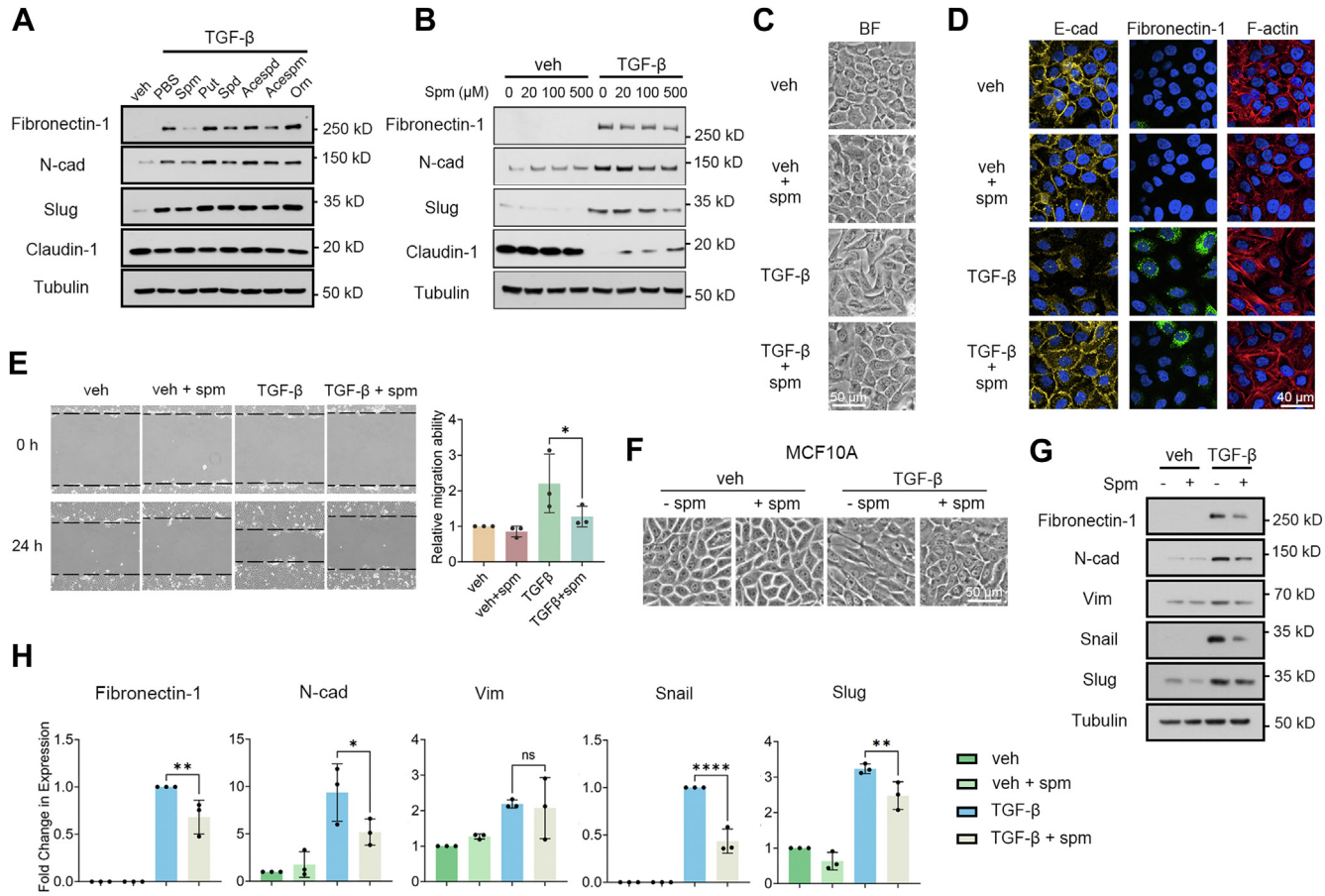

Figure 2. Spermine attenuates TGF-β-induced EMT. *A*, HaCaT cells were treated with 100 pM TGF-β along with 500 μM polyamines or polyamine-related metabolites for 24 h. EMT marker expression was examined by Western blot. Tubulin serves as a loading control. *B*, immunoblotting of EMT markers in HaCaT cells treated with vehicle or TGF-β with increased gradients of spermine for 24 h. *C*, HaCaT cells were treated with TGF-β and/or 500 μM spermine for 24 h and visualized with bright-field microscopy. *D*, HaCaT cells were treated with TGF-β and/or 500 μM spermine for 24 h and visualized by immunofluorescence. Representative fields are shown with equivalent projections. *E*, HaCaT cells were wounded with a tip and treated with TGF-β. Relative migration was calculated as the percentage of invaded area at time 24 h normalized to the vehicle control. Data are means ± SD from n = 3 independent experiments. $^{*}p < 0.05$, by one-way ANOVA with Sidak's test. *F*, bright-field images of MCF10A cells show mitigating effects of spermine on TGF-β-altered cell morphology. Cells were pretreated with 500 μM spermine for 16 h and then with vehicle or TGF-β for an additional 36 h. *G*, immunoblotting of EMT markers in MCF10A cells treated with or without 500 μM spermine for 16 h prior to the treatment of TGF-β for 36 h. *H*, qantification of relative EMT marker expression in (*G*). Data are means ± SD from n = 3 independent experiments. $^{**}p < 0.01$, $^{****}p < 0.0001$, by one-way ANOVA with Sidak's test. EMT, epithelial–mesenchymal transition; TGF-β, transforming growth factor-beta.

coated surface, we observed augmented EMT phenotypes in cells grown on FN compared with cells on Matrigel. Even in the absence of or with a minimal dosage of TGF-β, cells grown on FN had already displayed spindle-like morphology and prominent expression of N-cadherin, with claudin-1 levels slightly decreased (Figs. 4, *A* and *B*, and S4*A*). Intriguingly, these phenomena characteristic of increased EMT response were not observed in cells overexpressing FN-1 upon doxycycline induction (Fig. S4, *B* and *C*). This could be due to the inefficient assembly of excessively induced FN-1 into the matrix, as this process requires binding to specific integrin families (primarily α5β1) (54), which may be present at insufficient levels. In contrast, coated FN, as an immediate and bioactive substrate, can effectively interact with many more types of integrins to perform its function (54).

After verifying that the FN matrix could improve the cellular response to EMT, we tried to answer whether it was involved in spermine-mediated EMT alleviation. However, knocking down FN-1 to a level commensurate with that reduced by spermine did not reproduce the mitigating effects on EMT (Fig. S4*D*), implicating that a decrease in FN-1 levels alone was insufficient to curb the EMT process. On the other hand, the attenuating effects of spermine on EMT were partially rescued in cells grown on FN, as evidenced by the subdued reduction in FN-1 and Slug levels, along with an increased expression of N-cadherin (Fig. 4, *C* and *D*). Collectively, these findings indicate that FN-1 matrix is involved in the suppression of EMT by spermine and likely acts in coordination with other elements.

The TGF-β–extracellular signal–regulated kinase axis upregulates SMOX *to shrink the spermine pool*

We next attempted to explore how TGF-β signaling reduces the spermine level. By analyzing the gene expression profiles of polyamine metabolic enzymes, we discovered that TGF-β specifically and rapidly increased the expression of *SMOX* in HaCaT cells (Fig. 5*A*), which catalyzes the one-step conversion

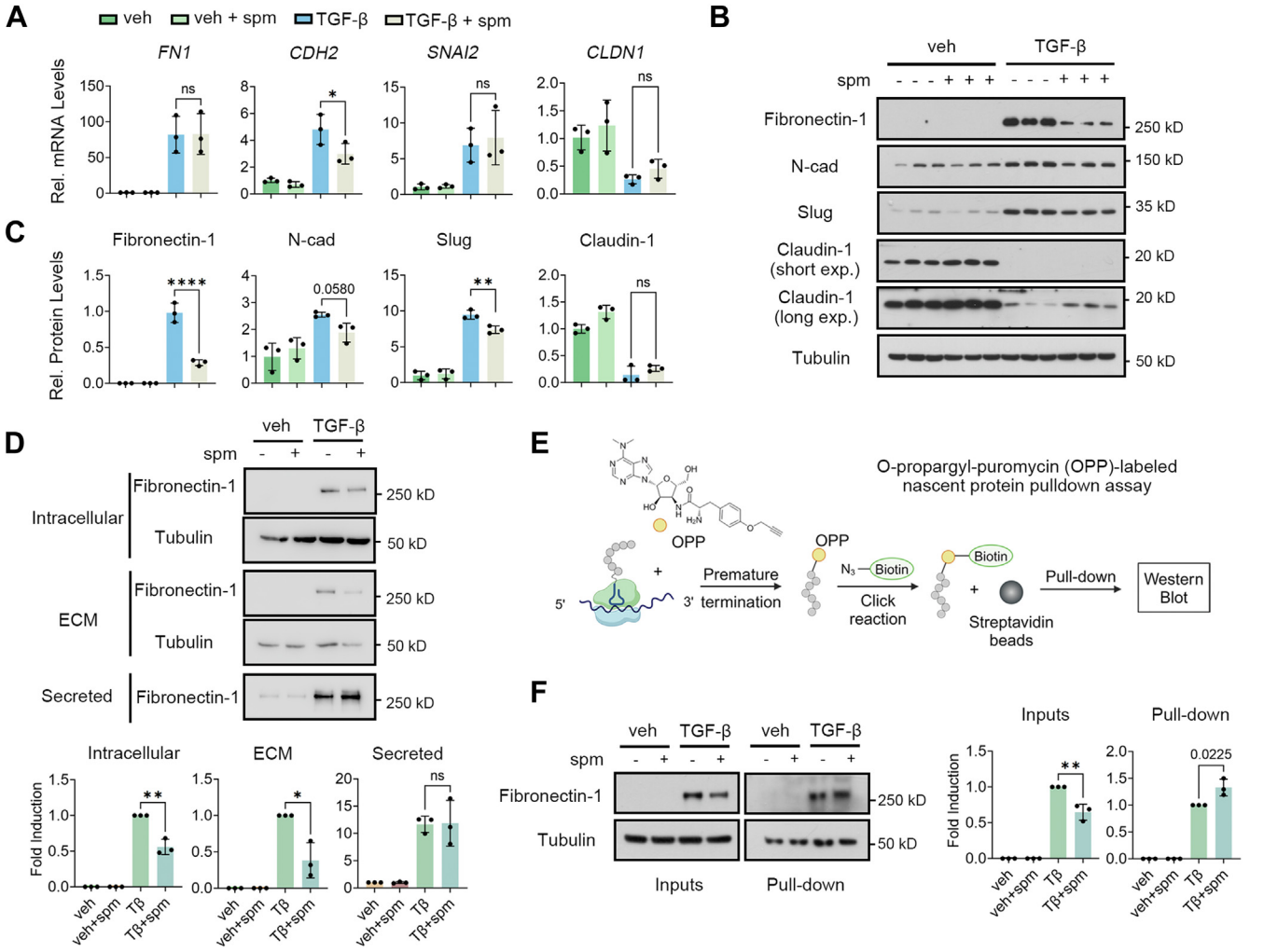

Figure 3. Spermine promotes fibronectin matrix reduction. *A* and *B*, HaCaT cells were treated with vehicle or 100 pM TGF-β with or without 500 μM spermine for 24 h. *A*, relative expression of EMT markers in each sample was examined at the mRNA level by quantitative RT–PCR normalized to *GAPDH*. Data are means ± SD from n = 3 independent experiments. ns, not significant, $^{*}p < 0.05$, by one-way ANOVA with Sidak's test. *B*, immunoblotting analysis of EMT marker expression. Tubulin serves as a loading control. *C*, relative expression of EMT marker proteins in (*B*) was quantified and normalized to tubulin. Data are means ± SD from n = 3 independent experiments. ns, not significant, $^{**}p < 0.01$, $^{****}p < 0.0001$, by one-way ANOVA with Sidak's test. *D*, HaCaT cells were treated with vehicle or TGF-β with or without 500 μM spermine for 24 h, and then the intracellular, ECM, and secreted content of fibronectin-1 was separately extracted for immunoblotting. Data are means ± SD from n = 3 independent experiments. ns, not significant, $^{*}p < 0.05$, $^{**}p < 0.01$, by one-way ANOVA with Sidak's test. *E*, a schematic representation of OPP-labeled nascent protein pull-down assay to examine protein synthesis by Western blot. *F*, determination of relative levels of newly synthesized fibronectin-1 of HaCaT cells treated with vehicle or TGF-β with or without 500 μM spermine for 24 h using the methods described in (*D*). Data are means ± SD from n = 3 independent experiments. $^{**}p < 0.01$, by one-way ANOVA with Sidak's test. EMT, epithelial–mesenchymal transition; OPP, O-propargyl-puromycin; TGF-β, transforming growth factor-beta.

of spermine to spermidine. This induction depended on TβRI kinase activity (Fig. 5*B*) but was SMAD4 independent, as cells with SMAD4 deletion still exhibited elevated *SMOX* mRNA levels following TGF-β treatment (Fig. 5, *C* and *D*), indicating a role of non-Smad TGF-β signaling pathways in regulating *SMOX* expression. To identify the noncanonical pathway responsible for the enhanced expression of *SMOX* by TGF-β, we first examined the phosphorylation levels of several key players downstream of TGF-β signaling. The activities of ERK (extracellular signal–regulated kinase), p38, and AKT were all activated by TGF-β in HaCaT cells and could be suppressed by specific inhibitors (Fig. S5*A*). Notably, only inhibition of ERK with SCH772984 or U0126 could significantly block the increased *SMOX* expression induced by TGF-β (Figs. 5*E* and S5*B*). These findings corroborate that TGF-β upregulates SMOX *via* the ERK–mitogen-activated protein kinase signaling pathway.

To validate that TGF-β-induced *SMOX* upregulation is accountable for spermine reduction, we generated monoclonal SMOX-KO HaCaT cells. Disruption of *SMOX* was validated at the gene level by the presence of indels that lead to frame-shifting mutations and resulting truncated protein products (Fig. 5*F*). RT–quantitative PCR (qPCR) primers targeting the disrupted gene sequence validated no expression of *SMOX* in the *SMOX*-deficient cells (Fig. 5, *G* and *H*). Importantly, *SMOX* depletion thwarted TGF-β-induced reduction in spermine concentration (Fig. 5*I*), upholding the important role of SMOX in reducing spermine levels during TGF-β-induced EMT.

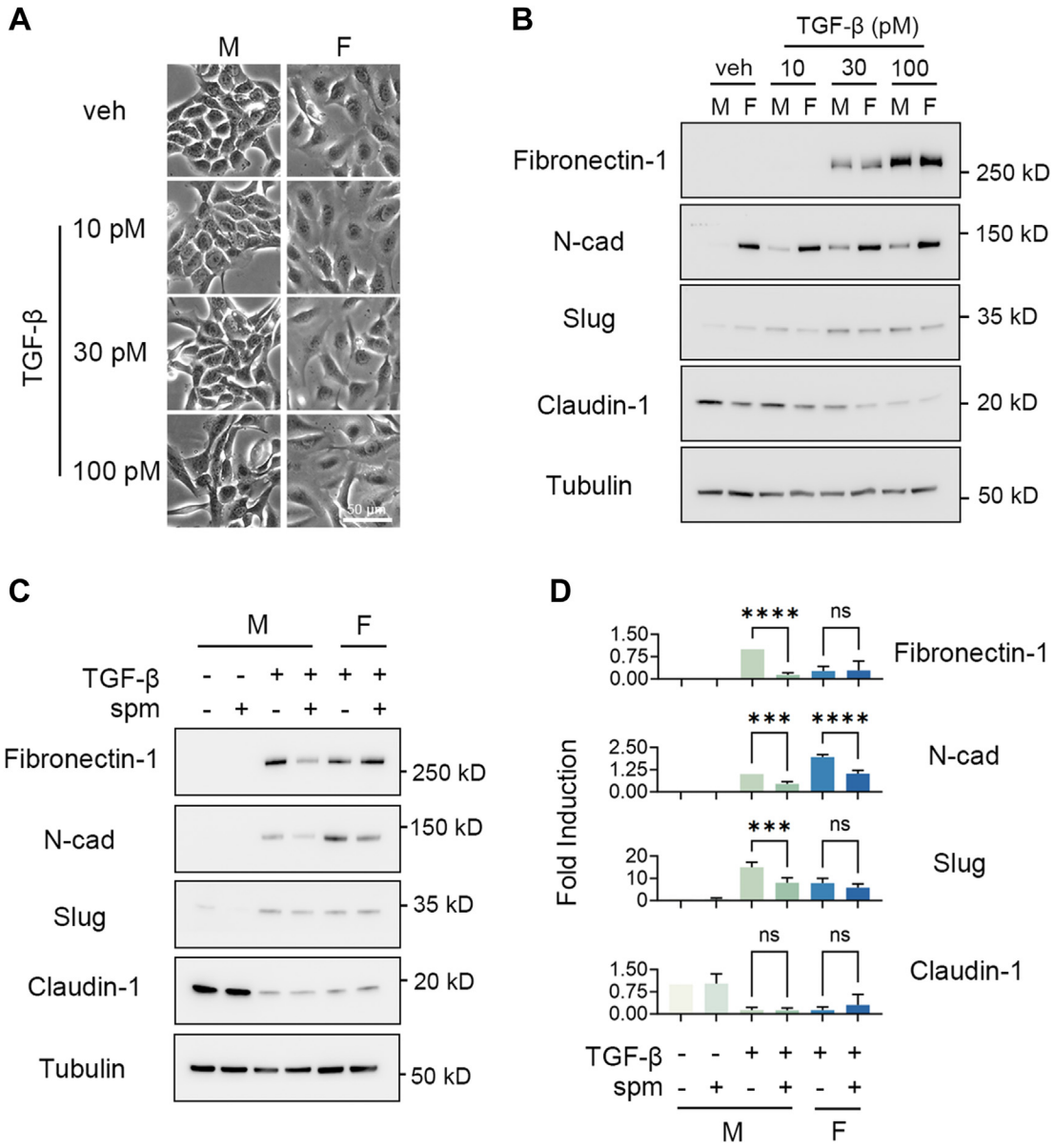

Figure 4. Fibronectin-1 restores the spermine-constrained EMT. *A*, morphological changes of HaCaT cells growing on Matrigel (M) or human serum plasma fibronectin (F) treated with increasing concentrations of TGF-β. *B*, HaCaT cells growing on Matrigel (M) or human serum plasma fibronectin (F) were treated with increasing concentrations of TGF-β, and expression of EMT markers was analyzed by immunoblotting. Tubulin serves as a loading control. *C*, immunoblotting analysis of spermine effects on EMT marker expression in HaCaT cells growing on surface with Matrigel (M) or fibronectin (F) coating. *D*, quantification of relative EMT marker expression in (*C*). Data are presented as mean ± SD from n = 3 independent experiments. ns, not significant, ***$p < 0.001$, ****$p < 0.0001$, by one-way ANOVA with Sidak's test. EMT, epithelial–mesenchymal transition; TGF-β, transforming growth factor-beta.

Discussion

TGF-β signaling has long been recognized as a potent inducer of EMT through a variety of mechanisms (9–13), yet whether TGF-β can induce the EMT program *via* metabolic reprogramming eludes close investigation. In the present study, we disclose that TGF-β upregulates SMOX expression *via* ERK, resulting in decreased endogenous spermine content during the early stages of EMT. Importantly, supplementation of spermine attenuates the EMT program and downregulates the expression of several key EMT markers primarily at the protein level, likely by promoting the degradation of the FN matrix.

EMT is a highly dynamic process intertwined with the remodeling of cell metabolism (55, 56). The progressive and plastic nature of the EMT spectrum suggests that differential metabolic patterns may occur in varying EMT conditions, either as byproducts or playing an active role in priming or sustaining a particular EMT stage. Hence, elucidation of metabolic changes that precede and prime EMT activation (57) could potentially provide novel therapeutic targets for the prevention of EMT program in diseases. The reduced cellular spermine levels and several other metabolic changes, such as arginine, proline, and aspartate metabolism, induced by TGF-β treatment might serve as an early metabolic signature that

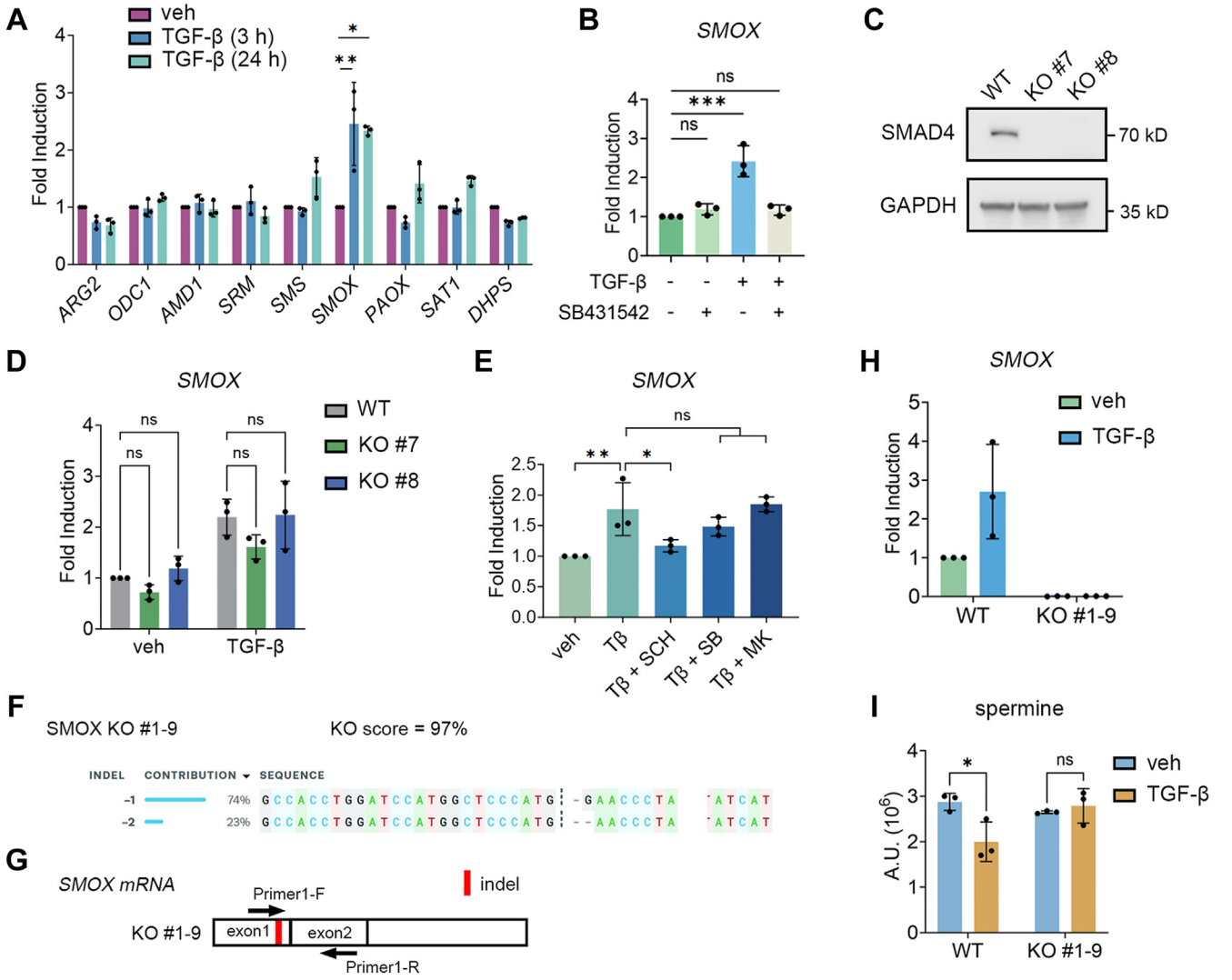

Figure 5. TGF-β engages ERK to upregulate *SMOX* that decreases spermine concentrations. *A*, relative expression of polyamine-associated genes in HaCaT cells following TGF-β treatment at different times was determined by quantitative RT–PCR (qRT–PCR) normalized to *GAPDH*. Data are means ± SD from n = 3 independent experiments. $*p < 0.05$, $**p < 0.01$, by one-way ANOVA with Sidak's test. *B*, relative expression of SMOX in HaCaT cells treated with 100 pM TGF-β for 3 h with or without a 21 h pretreatment with 10 μM SB431542. Data are means ± SD from n = 3 independent experiments normalized to *GAPDH*. ns, not significant, $***p < 0.001$, by one-way ANOVA with Dunnett's test. *C*, immunoblot validation of Smad4 KO in two clones of HaCaT cell lines. GAPDH serves as a loading control. *D*, relative expression of *SMOX* in Smad4-KO HaCaT cells treated with TGF-β for 24 h was determined by qRT–PCR normalized to *GAPDH*. Data are means ± SD from n = 3 independent experiments. ns, not significant, by two-way ANOVA with Sidak's test. *E*, HaCaT cells were serum-starved for 24 h and then pretreated with SCH772984 (SCH, 500 nM), SB203580 (SB, 10 μM), or MK2206 (MK, 5 μM) for 30 min prior to 3 h of TGF-β stimulation. Relative expression of *SMOX* was examined by qRT–PCR normalized to *GAPDH*. Data are means ± SD from n = 3 independent experiments. ns, not significant, $*p < 0.05$, $**p < 0.01$, by one-way ANOVA with Sidak's test. *F*, validation of *SMOX* gene disruption by Sanger sequencing. Edited sequences resulted in frame-shifting mutations. *G*, schematic representation of validating the presence of indels in *SMOX* mRNA by RT–qPCR. *H*, relative expression of *SMOX* in *SMOX*-KO monoclonal cell lines was determined by RT–qPCR using the primers described in (*G*) and was normalized to *GAPDH*. Data are means ± SD from n = 3 independent experiments. *I*, quantification of intracellular spermine levels in the WT and SMOX-KO cells treated with TGF-β for 24 h. Data are means ± SD from n = 3 biological replicates. ns, not significant, $*p < 0.05$, by two-way ANOVA with Sidak's test. ERK, extracellular signal–regulated kinase; TGF-β, transforming growth factor-beta.

contributes to EMT initiation. Although these findings were recorded in HaCaT cells, the observed similar attenuating effects of spermine on MCF10A cells, along with a previous finding that addition of a polyamine mixture to polyamine-depleted Madin–Darby canine kidney cells rescues EMT phenotypes (58), suggest a potential broad implication.

The polyamine metabolism is tightly controlled because of its functional importance in a broad range of cell activities, including cell proliferation, immune regulation, and autophagy (26, 59, 60). However, the molecular regulation of the polyamine metabolism by signaling pathways is not well studied (61). Our data establish that TGF-β signaling can downregulate the levels of individual polyamines and particularly decrease spermine concentrations *via* inducing SMOX expression during EMT. Consistent to our observation, a recent study reported that TGF-β increases SMOX production and decreases spermine concentration in the mouse tubular epithelial cell line (62). Of note, several early studies reported that TGF-β could inhibit the ODC1 and AMD1 activity in some cell lines without statistically reducing the overall

polyamine content (58, 63, 64). This inconsistency might be explained by different biological contexts in which the experiments were conducted.

An interesting finding of our study is that spermine rather than other polyamines or related derivatives exhibits obvious EMT-attenuating effects. Although polyamine molecules are similar in structure, they differ in the length of their backbones and the number of positively charged amine groups, potentially resulting in distinct functions. Indeed, spermidine and spermine have demonstrated greater functionality than the diamine putrescine in cellular physiology, particularly regarding their aging-slowing effects, while the function of the two higher polyamines is thought to be similar (59, 65). However, the effects of spermidine and spermine also manifest disparities in several aspects. For example, spermine is more effective than spermidine in stimulating DNA B to Z conversion or modulating functions of several protein kinases as well as ion channels (66). Spermine also binds to hydroxyl-CoA dehydrogenase more competitively than spermidine, leading to the blockade of spermidine activation of the enzyme and weakened fatty acid oxidation (30). Interestingly, spermidine instead of spermine promotes the interaction between the core clock repressors, PER2 and CRY1, thereby contributing to circadian rhythmicity (37). Understanding the structural basis of spermidine and spermine that underpin their functional differences will be an important topic.

Fibronectin is an ECM protein essential for ECM assembly and functions in the form of a fibrillar network when binding to cell surfaces (54). Our study discovers that spermine can downregulate the level of FN fibrils. This downregulation is not at the transcriptional level or translational level, suggesting that spermine diminishes the FN matrix through other mechanisms, such as slowing its assembly or promoting its degradation. How intracellular spermine can affect the extracellular FN matrix needs future investigation.

In summary, our findings describe a TGF-β-induced reduction in spermine concentration as an early metabolic signature of EMT and demonstrate the function of spermine in EMT suppression. Considering that spermine is abundant in the daily nutrition of humans owing to its ubiquitous presence in living organisms and heat resistance (65), it opens the possibility of developing dietary supplementation of spermine as an adjuvant to facilitate the treatment of EMT-associated diseases like fibrosis.

Experimental procedures

Cell culture

All cell lines used in this study were from American Type Culture Collection or National Collection of Authenticated Cell Cultures and routinely tested for mycoplasma free. HaCaT cells were cultured in DMEM (Corning; catalog no.: 10-013-CMR) supplemented with 10% FBS (ExCell; catalog no.: FND500). MCF10A cells were cultured in DMEM/F12 medium (Corning; catalog no.: 10-092-CV) supplemented with 5% donor equine serum (Hyclone; catalog no.: SH30074.03), 20 ng/ml EGF (Novoprotein; catalog no.: C029), 500 ng/ml hydrocortisone (Macgene; catalog no.: CC103), 10 μg/ml insulin (Selleck; catalog no.: S6955), and 100 ng/ml cholera toxin (Macgene; catalog no.: CC104). 1X penicillin/streptomycin (Gibco; catalog no.: 15140122) was routinely added to the medium to prevent contamination. 100 pM or 400 pM TGF-β1 (Novoprotein; catalog no.: CA59) was used to induce EMT in HaCaT and MCF10A cells, respectively, unless indicated otherwise. Polyamine assays were all conducted in low-serum media (0.2% FBS) or serum-free media to minimize the effects of serum amine oxidases (67) unless indicated otherwise. To coat the tissue culture plates, wells were incubated with 20 μg/ml Matrigel (Corning; catalog no.: 356231) or human plasma FN (Solarbio; catalog no.: F8180) in PBS at 4 °C overnight.

Antibodies and reagents

The primary antibodies used in this study were anti-FN-1 (BD; catalog no.: 610077), anti-E-cadherin (CST; catalog no.: 3195), anti-N-cadherin (BD; catalog no.: 610920), anti-Slug (CST; catalog no.: 9585), anti-Snail (CST; catalog no.: 3879), antivimentin (CST; catalog no.: 5741), anti-claudin-1 (Santa; catalog no.: sc-166338), anti-GAPDH (ZSGB; catalog no.: TA-08), antitubulin (ZSGB; catalog no.: TA-10), anti-p-ERK (Santa; catalog no.: sc-7383), anti-ERK (Santa; catalog no.: sc-93), anti-p-p38 (CST; catalog no.: 9215), anti-p38 (Santa; catalog no.: sc-7972), anti-p-AKT (CST; catalog no.: 4060), anti-AKT (CST; catalog no.: 9272), anti-eIF5A (Abcam; catalog no.: ab32443), anti-eIF5A^{H} (AtaGenix; catalog no.: ATMA10343Mo), and anti-Smad4 (CST; catalog no.: 46535). The secondary antibodies used were horseradish peroxidase (HRP)–conjugated-anti-rabbit IgG (Invitrogen; catalog no.: 31460), HRP-conjugated anti-mouse IgG (Invitrogen; catalog no.: 31430), Alexa Fluor 488 antimouse IgG (Jackson; catalog no.: 715-545-150), and Alexa Fluor 647 anti-rabbit IgG (Jackson; cataog no.: 711-605-152).

The following compounds were used: GC7 (MCE; catalog no.: HY-108314A), putrescine (Macklin; catalog no.: D806929), spermidine (Sigma; catalog no.: 85578), spermine (Sigma; catalog no.: 85605), N1-acetyl-spermidine (Bidepharm; catalog no.: BD251323), N1-acetylspermine (Sigma; catalog no.: 01467), ornithine (Solarbio; catalog no.: O8070), SB431542 (Selleck; catalog no.: S1067), SCH772984 (MCE; catalog no.: HY-50846), U0126 (MCE; catalog no.: HY-12031), SB-203580 (MCE; catalog no.: HY-10256A), MK-2206 (MCE; catalog no.: HY-10358), and aminoguanidine (MCE; catalog no.: HY-B1041).

Cell proliferation assay

Adherent cells were dissociated into single cells and mixed 1:1 with the Trypan Blue solution (Gibco; catalog no.: 15250061). Cell number was counted using Countess 3 automated cell counter (Invitrogen) or CellDrop BF (DeNovix).

Wound healing assay

The confluent cell monolayer in a 12-well plate was uniformly wounded by manually scraping the cells with a 200 μl pipette tip with the aid of a ruler. After washing with PBS three

times, cells were refed with low-serum medium (0.2% FBS) supplemented with TGF-β in the presence or the absence of spermine. Wound closure of migrating cells was photographed at time 0 and 24 h, respectively. The percentage of surface area invaded by cells was quantified by comparing the average area of the wounded surface from three different fields of view at time 24 h to time 0 using ImageJ software (https://imagej.net/ij/) and was normalized to the vehicle control to calculate the relative migration ability.

Cell transfection

Transfection of plasmid DNA into HaCaT cells was performed using Lipofectamine 2000 (Invitrogen; catalog no.: 11668027) or by electroporation. For chemical transfection, cells were plated and allowed to reach 70 to 80% confluence overnight. Lipofectamine 2000 was diluted with prewarmed Opti-MEM (Gibco; catalog no.: 31985070), incubated for 5 min at room temperature, and then added to Opti-MEM containing targeted plasmid DNA (Lipofectamine [μl]/DNA [ng] ratio = 3:1). After 20 min of incubation at room temperature, the liposome–DNA mixture was added dropwise to the cells refed with fresh medium and incubated for 18 h.

For electroporation, cells grown to 70 to 80% confluence were trypsinized, washed three times with Opti-MEM, and suspended in Opti-MEM without antibiotics. Vectors were transfected into 2×10^6 cells (100 μl) using the Super Electroporator NEPA21 Type II (NEPAGENE) and a 175 V:5 ms:2 pulse program.

Lentivirus production and transduction

Lentiviruses were produced by cotransfection of 5 μg psPAX2 (Addgene; catalog no.: 12260), 5 μg pMD2.G (Addgene; catalog no.: 12259), and 10 μg expression plasmids with 60 μg polyethyleneimine (sigma) into 293FT cells cultured in 10 cm dish. After 6 h, the medium was refreshed. The virus-containing supernatant was collected and pooled 24 h and 48 h post-transfection and passed through a 0.45 μm filter (Millipore; catalog no.: SLHVR33RB) to eliminate cell debris. Viruses were then concentrated through centrifugation at 1600*g* for 1 h at 4 °C after adding PEG-8000 (Sigma; catalog no.: 89510) solution to the medium to a final concentration of 10% (w/v). The pellet was resuspended using approximately 500 μl DMEM and aliquoted and stored at −80 °C until use. For lentivirus transduction, cells were seeded 2×10^5 cells per well in a 6-well plate and infected in 1.5 ml medium containing 10 μg/ml polybrene (Beyotime; catalog no.: C0351) and an appropriate volume of concentrated viruses for 36 h.

Cell line construction

For CRISPR–Cas9-mediated *SMOX*-KO, we designed by CHOPCHOP the sgRNA: 5′-ATGATAGATAGGGTTCCCAT-3′ targeting the *SMOX* open reading frame and cloned them into the pX458 plasmid (Addgene; catalog no.: 48138). For CRISPR–Cas9-mediated *SMAD4*-KO, the sgRNA 5′-TGATCTATGCCCGTCTCTGG-3′ was used. HaCaT cells were transfected with the plasmid DNA by electroporation. After 48 h, single GFP^+ cells were sorted into 96-well plates for clonal expansion. Monoclonal cells with *SMOX* KO were validated at the gene level by Sanger sequencing and at the mRNA level by RT–qPCR, whereas cells with *SMAD4* deletion were validated at the protein level.

For shRNA knockdown of *FN1*, the shRNA 5′-TGCAGCACAACTTCGAATTAT-3′ was cloned into the pLKO.5-puro plasmid (Merck; catalog no.: SHC201) and packaged into lentiviruses. HaCaT cells were then infected, and stable cell lines were selected by 1 μg/ml puromycin (Gibco; catalog no.: A1113803) for 3 days. *FN1* knockdown was validated at the protein level.

To generate TetON-FN1 stable HaCaT cells, a ∼7 kb coding sequence of FN1 (V89) was amplified from the complementary DNA (cDNA) by PCR using PrimeSTAR Max DNA Polymerase (Takara; catalog no.: R045A) and cloned into the pCW57.1 plasmid (gifted by S. Ding, Tsinghua University). The vector was then packaged into lentiviruses and transfected into HaCaT cells. Stable cell lines were selected by 1 μg/ml puromycin for 3 days. Doxycycline induction of FN-1 expression was validated at the protein level.

Luciferase reporter assay

HaCaT cells were seeded into 6- or 12-well plates and were allowed to reach 80% confluence overnight. About 2 μg (6-well) or 1 μg (12-well) of pGL3-CAGA-luc plasmid and 200 ng (6-well) or 100 ng (12-well) of Renilla internal control plasmid were cotransfected into HaCaT cells by Lipofectamine 2000. After 18 h incubation, cells were dissociated and plated into 24-well plates in triplicate. Cells were treated with spermine after 6 h and stimulated with different concentrations of TGF-β for 24 h to induce luciferase expression. The luciferase activity was measured by a Centro LB 960 Microplate Luminometer (Berthold Technologies) using the Dual-Luciferase Reporter Assay System (Promega) and was normalized to the cotransfected Renilla activity.

Immunofluorescence

Cells growing on the glass coverslip were washed two times with PBS and fixed with 4% paraformaldehyde for 15 min. The cells were then washed three times with PBS and permeabilized and blocked in 3% bovine serum albumin (0.3% Triton X-100 in PBS) for 1 h. All the procedures were performed at room temperature. After blocking, cells were incubated with primary antibodies diluted 1:500 in 3% bovine serum albumin (0.3% Triton X-100 in PBS) overnight at 4 °C, washed three times with PBS for 10 min, and finally incubated with appropriate secondary antibodies (1:500 dilution) and 4′,6-diamidino-2-phenylindole (1:1000 dilution) plus Phalloidin-iFluor 555 Conjugate (1:1000 dilution; AAT Bioquest) for 1 h at room temperature in the dark. The coverslips were then washed three times with PBS for 10 min and mounted onto glass slides with a drop of antifade mounting medium (2.5% DABCO and 40% glycerol in PBS). The samples were photographed using an Olympus FV3000 confocal microscope.

Protein extraction and immunoblotting

Cells were washed once with PBS and lysed in radioimmunoprecipitation assay buffer (Beyotime; catalog no.: P0013C) supplemented with protease and phosphatase inhibitors on ice for 10 min. Proteins were then collected from the supernatant of cell lysates after centrifugation at 16,000*g* for 5 min at 4 °C. Total protein concentration was determined by bicinchoninic acid (BCA) assay. Denatured protein was loaded for separation by SDS-PAGE and transferred onto 0.2 μm nitrocellulose membrane. Membranes were blocked in 5% nonfat milk in TBST (Tris-buffered saline with Tween-20) at room temperature for 1 h, followed by incubation with the indicated primary antibodies diluted 1:1000 at 4 °C overnight. After incubation, membranes were washed three times with TBST for 10 min, incubated with appropriate secondary HRP-conjugated antibodies (1:1000 dilution) at room temperature for 1 h, and washed another three times with TBST for 10 min. Immunolabeled target proteins were detected using SuperSignal West Pico PLUS Chemiluminescent Substrate (Thermo; catalog no.: 34580) by X-ray film (Kodak) or the MiniChemi Mini Chemiluminescent/Fluorescent Imaging and Analysis System (SinSage). The blots without oversaturation were quantified by GelAnalyzer 23.1.1 software (http://www.gelanalyzer.com/?i=1), and targeted protein levels were normalized to tubulin.

OPP-labeled nascent FN-1 protein pull-down and analysis

The level of newly synthesized FN-1 was analyzed as described previously (68) with some modifications. To label nascent proteins, 30 μM OPP (MCE; catalog no.: HY-15680) was added to the medium for 3 h before sample collection. Cells were washed once with PBS and lysed in radioimmunoprecipitation assay buffer containing 1 mM PMSF. The protein lysates were mixed with Biotin Azide Plus (Click Chemistry Tools; catalog no.: 1488) and click-reacted using the Click-&-Go Protein Reaction Buffer Kit (Click Chemistry Tools; catalog no.: 1262) following the provided instruction to allow conjugation of OPP-tagged protein with biotin azide. After click reaction, proteins were precipitated by five volumes of cold acetone overnight at −20 °C. Precipitated proteins were centrifuged at 4000*g* at 4 °C for 10 min, and the pellets were washed twice with 1 ml of cold methanol with vortex until the color turned light yellow. The pellets were then air-dried for 15 min and reconstituted with 1% SDS in PBS. Protein concentration was determined by BCA assay, and 30 μg of protein was saved as input control. The concentration of SDS in protein lysates was then diluted to 0.1% by PBS, and 150 μg of protein was incubated with high-capacity streptavidin magnetic beads (Click Chemistry Tools; catalog no.: 1497-1) overnight at 4 °C with slow rotation on a plastic rotator. After incubation, the beads were washed thrice with 1 ml PBS containing 1% NP-40 and 0.1% SDS at 4 °C for 5 min with slight rotation and were boiled at 95 °C in 1X Laemmli sample buffer for 10 min to elute labeled nascent proteins for Western blotting. Relative levels of total and nascent FN-1 were determined by normalizing input levels and the pull-down to tubulin, respectively.

DOC extraction of cell lysates

The intracellular, fibrillar, and secreted FN-1 fractions were differentially extracted as described previously (69). Cells growing on 12-well plates were washed with PBS once, lysed with DOC buffer (2% DOC, 2 mM Tris–HCl, pH 8.8, 2 mM EDTA, 2 mM iodoacetic acid, and 2 mM *N*-ethyl-maleimide) containing 2 mM PMSF for 10 min on ice and then passed through a 26-gauge syringe and centrifuged at 4 °C, 20,000*g* for 20 min. The clear supernatant was collected and kept as the soluble FN fraction (intracellular), whereas the pellet was washed with DOC buffer and centrifuged again to obtain the final pellet containing the cross-linked (fibrillar) FN matrix, which was resuspended in 1% SDS (25 mM Tris–HCl, pH 8.0, 2 mM EDTA, 2 mM iodoacetic acid, and 2 mM *N*-ethyl-maleimide). To determine secreted FN1 concentration, the culture medium was centrifugated at 12,000*g* for 5 min to pellet cell debris. The protein content in the supernatant was precipitated by 20% trichloroacetic acid (TCA) at 4 °C overnight and pelleted by centrifugation at 4 °C, 20,000*g* for 20 min. The pellet was then washed with cold acetone thrice, air dried, and reconstituted in 8 M urea (100 mM Tris–HCl, pH 8.8). The samples were boiled with 1X Laemmli buffer, and 15 μg of the DOC-soluble, the whole DOC-insoluble, and 15 μg of medium fractions were loaded for SDS-PAGE. Separated proteins were transferred onto a nitrocellulose membrane and processed with antibodies. Cellular FN1 levels were quantified by GelAnalyzer 23.1.1 software and normalized to tubulin levels, whereas secreted FN1 levels were directly normalized to the vehicle control. Protein concentration was quantified by a BCA assay.

RNA extraction and RT–qPCR

Total RNA was extracted using the M5 Universal Plus RNA mini Kit (Mei5Bio; catalog no.: MF167-01) according to the manufacturer's guide. cDNAs were generated using the HiScript II first Strand cDNA Synthesis Kit (Vazyme; catalog no.: R211-01). RT–qPCR was performed with 10 ng cDNA samples and 200 nM of each primer using NovoStart SYBR qPCR SuperMix Plus (Novoprotein; catalog no.: E096-01A) in the 96/384-well plate format in the LightCycler 480 (Roche) or QuantStudio 6 Pro (Applied Biosystems) systems. Relative mRNA levels were calculated using the $2^{-\Delta\Delta Cq}$ method and normalized to *GAPDH* mRNA. The primers used are listed in Table S1.

Untargeted metabolomics analysis

Cellular metabolites were extracted as described previously (70) with some modifications. Cells growing on 100 mm dishes were washed with cold PBS three times and lysed in 1 ml prechilled 80% (v/v) methanol (−80 °C, HPLC grade) on dry ice followed by incubation at −80 °C for 1 h. The cell lysate–methanol mixture was scraped to a 2 ml Eppendorf tube on dry ice. An additional 500 μl of 80% (v/v) methanol was then added to the dish, and the resulting mixture was combined in the same tube. The metabolite-containing fraction was obtained by centrifuging the mixture at 14,000*g* at 4 °C for 20 min and was dried by a SpeedVac Concentrator.

Reconstituted sample volumes were normalized to the total cellular protein concentration.

Q Exactive orbitrap mass spectrometer coupled with Ultimate 3000 UHPLC system (Thermo Fisher Scientific) was used in metabolomics analysis. Data-dependent tandem mass spectrometry (MS/MS) acquisition with top 10 most intense precursors selected for fragmentation was applied in data acquisition. Mass resolutions of 70,000 and 17,500 were set for MS and MS/MS scans, respectively. In positive ion mode, the BEH amide column (2.1 mm × 100 mm; Waters) was used with mobile phases containing ammonium acetate in 95% and 50% acetonitrile. BEH C18 column (2.1 mm × 100 mm; Waters) was used for analysis in negative ion mode. Aqueous phase with ammonium acetate and acetonitrile was prepared as mobile phases for the reverse phase column.

Metabolites were identified and quantified using Tracefinder 3.2 ((Thermo Fisher Scientific) with an in-house library containing MS/MS spectra from over 1500 endogenous metabolites. Metabolites were assigned based on accurate precursor masses and fragment matching with MS/MS spectra in the library. Mass tolerance of 10 and 15 ppm was applied for precursor and fragment search. The chromatographic peak area was used for relative quantitation. Retention time shift of 0.25 min was allowed for peak alignment. Metabolic differential analysis was carried out by MetaboAnalyst (https://www.metaboanalyst.ca/MetaboAnalyst/home.xhtml).

Extraction and detection of polyamines

Polyamine extraction was performed as described previously (71) with small modifications. For cellular polyamine extraction, cells growing on 6-well plates were washed three times with cold PBS. After washing, cells were scraped and suspended in 200 μl cold PBS. The cell–PBS mixture was treated with 100 μl of 50% (v/v) TCA and centrifuged at 12,000*g* at 4 °C for 2 min to precipitate the cell debris and proteins. The resulting supernatant was then neutralized with 2 ml of 2 M NaOH and reacted with 10 μl of 50% (v/v) benzoyl chloride (in methanol) with continuous shaking at 220 rpm at room temperature for up to 2 h. Benzoylated polyamines were subsequently extracted using two sequential chloroform extractions. The chloroform layer was dried using a stream of nitrogen. Reconstituted sample volumes were normalized to the total cellular protein concentration. For medium polyamine extraction, 1 ml of medium was first centrifuged at 12,000*g* at 4 °C for 5 min to remove cell debris. The supernatant was then treated with 100 μl of 50% (v/v) TCA and 50 pM internal standard (1,8-diaminooctane) prior to downstream applications. Derivatized polyamines were analyzed using TSQ Quantiva ((Thermo Fisher Scientific). Ion transitions +297.2/+105.2, +458.3/+336.2, +619.3/+497.2, and +353.2/+104.9 were applied for putrescine, spermidine, spermine, and internal standard. BEH C18 column (2.1 × 50 mm, 1.7 μm; Waters) was used in the analysis with mobile phase A containing 0.01% formic acid in aqueous and mobile phase B containing 0.01% formic acid in acetonitrile.

Statistical analysis

Statistical analysis was conducted using Prism 10 (GraphPad Software). For the comparison of multiple groups, one- or two-way ANOVA followed by Dunnett's or Sidak's multiple comparisons test was employed, focusing on the selected groups. For comparisons between two groups, the unpaired Student's *t* test or unpaired multiple *t* tests were utilized. The data were presumed to be parametric, and all statistical tests were two-tailed with a significance threshold set at $p < 0.05$.

Data availability

Data are available from the corresponding author upon reasonable request.

Supporting information—This article contains supporting information.

Acknowledgments—We thanked Dr Xiaohui Liu (Facility Center of Metabolomics and Lipidomics, National Center for Protein Sciences, Tsinghua University) for the metabolomics data curation and discussion. We thanked Dr Peng Jiang, Junxiu Nong, Qiaoni Shi, and Kexin Kang for insightful comments on the experiments. Illustrative figures were created using BioRender.

Author contributions—H. L. and Y.-G. C. conceptualization; H. L. methodology; H. L. software; H. L. formal analysis; H. L. investigation; H. L. and Y.-G. C. writing–original draft; H. L. and Y.-G. C. writing–review & editing; H. L. visualization; Y.-G. C. supervision; Y.-G. C. project administration; Y.-G. C. funding acquisition.

Funding and additional information—The study was supported by grants from the National Key Research and Development Program of China (grant no.: 2023YFA1800603), the Shenzhen Medical Research Fund (grant no.: B2302022), and Beijing Science and Technology Plan (grant no.: Z231100007223006), and the Natural Science Foundation of Jiangxi Province (grant no.: 20224ACB209001) to Y. G. C.

Conflict of interest—The authors declare that they have no conflicts of interest with the contents of this article.

Abbreviations—The abbreviations used are: BCA, bicinchoninic acid; cDNA, complementary DNA; DMEM, Dulbecco's modified Eagle's medium; DOC, deoxycholic acid; EMT, epithelial–mesenchymal transition; FBS, fetal bovine serum; FN, fibronectin; HRP, horseradish peroxidase; MS/MS, tandem mass spectrometry; OPP, O-propargyl-puromycin; qPCR, quantitative PCR; SMOX, spermine oxidase; TBST, Tris-buffered saline with Tween-20; TCA, trichloroacetic acid; TGF-β, transforming growth factor-beta.

References

1. Thiery, J. P., Acloque, H., Huang, R. Y. J., and Nieto, M. A. (2009) Epithelial-mesenchymal transitions in development and disease. *Cell* **139**, 871–890
2. Nieto, M. A. (2011) The ins and outs of the epithelial to mesenchymal transition in health and disease. *Annu. Rev. Cell Dev. Biol.* **27**, 347–376
3. Nieto, M. A., Huang, R. Y.-J., Jackson, R. A., and Thiery, J. P. (2016) Emt: 2016. *Cell* **166**, 21–45

4. Yang, J., Antin, P., Berx, G., Blanpain, C., Brabletz, T., Bronner, M., *et al.* (2020) Guidelines and definitions for research on epithelial–mesenchymal transition. *Nat. Rev. Mol. Cell Biol.* **21**, 341–352
5. Lambert, A. W., and Weinberg, R. A. (2021) Linking EMT programmes to normal and neoplastic epithelial stem cells. *Nat. Rev. Cancer* **21**, 325–338
6. Gonzalez, D. M., and Medici, D. (2014) Signaling mechanisms of the epithelial-mesenchymal transition. *Sci. Signal* **7**, re8
7. Lamouille, S., Xu, J., and Derynck, R. (2014) Molecular mechanisms of epithelial-mesenchymal transition. *Nat. Rev. Mol. Cell Biol.* **15**, 178–196
8. Dongre, A., and Weinberg, R. A. (2019) New insights into the mechanisms of epithelial-mesenchymal transition and implications for cancer. *Nat. Rev. Mol. Cell Biol.* **20**, 69–84
9. Heldin, C. H., Vanlandewijck, M., and Moustakas, A. (2012) Regulation of EMT by TGFbeta in cancer. *FEBS Lett.* **586**, 1959–1970
10. Katsuno, Y., Lamouille, S., and Derynck, R. (2013) TGF-beta signaling and epithelial-mesenchymal transition in cancer progression. *Curr. Opin. Oncol.* **25**, 76–84
11. Moustakas, A., and Heldin, C. H. (2016) Mechanisms of TGFbeta-induced epithelial-mesenchymal transition. *J. Clin. Med.* **5**, 63
12. Hao, Y., Baker, D., and Ten Dijke, P. (2019) TGF-beta-Mediated epithelial-mesenchymal transition and cancer metastasis. *Int. J. Mol. Sci.* **20**, 2767
13. Katsuno, Y., and Derynck, R. (2021) Epithelial plasticity, epithelial-mesenchymal transition, and the TGF-beta family. *Dev. Cell* **56**, 726–746
14. Li, X., Egervari, G., Wang, Y., Berger, S. L., and Lu, Z. (2018) Regulation of chromatin and gene expression by metabolic enzymes and metabolites. *Nat. Rev. Mol. Cell Biol.* **19**, 563–578
15. Rinschen, M. M., Ivanisevic, J., Giera, M., and Siuzdak, G. (2019) Identification of bioactive metabolites using activity metabolomics. *Nat. Rev. Mol. Cell Biol.* **20**, 353–367
16. Xu, D., Shao, F., Bian, X., Meng, Y., Liang, T., and Lu, Z. (2021) The evolving landscape of noncanonical functions of metabolic enzymes in cancer and other pathologies. *Cell Metab.* **33**, 33–50
17. Baker, S. A., and Rutter, J. (2023) Metabolites as signalling molecules. *Nat. Rev. Mol. Cell Biol.* **24**, 355–374
18. Morandi, A., Taddei, M. L., Chiarugi, P., and Giannoni, E. (2017) Targeting the metabolic reprogramming that controls epithelial-to-mesenchymal transition in aggressive tumors. *Front. Oncol.* **7**, 40
19. Sciacovelli, M., and Frezza, C. (2017) Metabolic reprogramming and epithelial-to-mesenchymal transition in cancer. *FEBS J.* **284**, 3132–3144
20. Dong, C., Yuan, T., Wu, Y., Wang, Y., Fan, T. W., Miriyala, S., *et al.* (2013) Loss of FBP1 by Snail-mediated repression provides metabolic advantages in basal-like breast cancer. *Cancer Cell* **23**, 316–331
21. Jiang, L., Xiao, L., Sugiura, H., Huang, X., Ali, A., Kuro-o, M., *et al.* (2015) Metabolic reprogramming during TGFbeta1-induced epithelial-to-mesenchymal transition. *Oncogene* **34**, 3908–3916
22. Sciacovelli, M., Goncalves, E., Johnson, T. I., Zecchini, V. R., da Costa, A. S., Gaude, E., *et al.* (2016) Fumarate is an epigenetic modifier that elicits epithelial-to-mesenchymal transition. *Nature* **537**, 544–547
23. Shaul, Y. D., Freinkman, E., Comb, W. C., Cantor, J. R., Tam, W. L., Thiru, P., *et al.* (2014) Dihydropyrimidine accumulation is required for the epithelial-mesenchymal transition. *Cell* **158**, 1094–1109
24. Holbert, C. E., Cullen, M. T., Casero, R. A., Jr., and Stewart, T. M. (2022) Polyamines in cancer: integrating organismal metabolism and antitumour immunity. *Nat. Rev. Cancer* **22**, 467–480
25. Casero, R. A., Jr., Murray Stewart, T., and Pegg, A. E. (2018) Polyamine metabolism and cancer: treatments, challenges and opportunities. *Nat. Rev. Cancer* **18**, 681–695
26. Gerner, E. W., and Meyskens, F. L., Jr. (2004) Polyamines and cancer: old molecules, new understanding. *Nat. Rev. Cancer* **4**, 781–792
27. Xu, H., Zhang, X., Wang, X., Li, B., Yu, H., Quan, Y., *et al.* (2024) Cellular spermine targets JAK signaling to restrain cytokine-mediated autoimmunity. *Immunity.* **57**, 1796–1811.e8
28. Zhao, C., Ma, Y., Zhang, M., Gao, X., Liang, W., Qin, Y., *et al.* (2023) Polyamine metabolism controls B-to-Z DNA transition to orchestrate DNA sensor cGAS activity. *Immunity* **56**, 2508–2522.e2506
29. Hibino, S., Eto, S., Hangai, S., Endo, K., Ashitani, S., Sugaya, M., *et al.* (2023) Tumor cell-derived spermidine is an oncometabolite that suppresses TCR clustering for intratumoral CD8(+) T cell activation. *Proc. Natl. Acad. Sci. U. S. A.* **120**, e2305245120
30. Al-Habsi, M., Chamoto, K., Matsumoto, K., Nomura, N., Zhang, B., Sugiura, Y., *et al.* (2022) Spermidine activates mitochondrial trifunctional protein and improves antitumor immunity in mice. *Science* **378**, eabj3510
31. Wagner, A., Wang, C., Fessler, J., DeTomaso, D., Avila-Pacheco, J., Kaminski, J., *et al.* (2021) Metabolic modeling of single Th17 cells reveals regulators of autoimmunity. *Cell* **184**, 4168–4185.e4121
32. Puleston, D. J., Baixauli, F., Sanin, D. E., Edwards-Hicks, J., Villa, M., Kabat, A. M., *et al.* (2021) Polyamine metabolism is a central determinant of helper T cell lineage fidelity. *Cell* **184**, 4186–4202.e4120
33. Zhang, H., Alsaleh, G., Feltham, J., Sun, Y., Napolitano, G., Riffelmacher, T., *et al.* (2019) Polyamines control eIF5A hypusination, TFEB translation, and autophagy to reverse B cell senescence. *Mol. Cell* **76**, 110–125.e119
34. Anderson-Baucum, E., Pineros, A. R., Kulkarni, A., Webb-Robertson, B. J., Maier, B., Anderson, R. M., *et al.* (2021) Deoxyhypusine synthase promotes a pro-inflammatory macrophage phenotype. *Cell Metab.* **33**, 1883–1893.e1887
35. Medina, C. B., Mehrotra, P., Arandjelovic, S., Perry, J. S. A., Guo, Y., Morioka, S., *et al.* (2020) Metabolites released from apoptotic cells act as tissue messengers. *Nature* **580**, 130–135
36. Eisenberg, T., Abdellatif, M., Schroeder, S., Primessnig, U., Stekovic, S., Pendl, T., *et al.* (2016) Cardioprotection and lifespan extension by the natural polyamine spermidine. *Nat. Med.* **22**, 1428–1438
37. Zwighaft, Z., Aviram, R., Shalev, M., Rousso-Noori, L., Kraut-Cohen, J., Golik, M., *et al.* (2015) Circadian clock control by polyamine levels through a mechanism that declines with age. *Cell Metab.* **22**, 874–885
38. Eisenberg, T., Knauer, H., Schauer, A., Buttner, S., Ruckenstuhl, C., Carmona-Gutierrez, D., *et al.* (2009) Induction of autophagy by spermidine promotes longevity. *Nat. Cell Biol.* **11**, 1305–1314
39. Murthy, D., Attri, K. S., Shukla, S. K., Thakur, R., Chaika, N. V., He, C., *et al.* (2024) Cancer-associated fibroblast-derived acetate promotes pancreatic cancer development by altering polyamine metabolism via the ACSS2-SP1-SAT1 axis. *Nat. Cell Biol.* **26**, 613–627
40. Guo, Y., Ye, Q., Deng, P., Cao, Y., He, D., Zhou, Z., *et al.* (2020) Spermine synthase and MYC cooperate to maintain colorectal cancer cell survival by repressing Bim expression. *Nat. Commun.* **11**, 3243
41. Guan, F., Handa, K., and Hakomori, S.-i. (2009) Specific glycosphingolipids mediate epithelial-to-mesenchymal transition of human and mouse epithelial cell lines. *Proc. Natl. Acad. Sci.* **106**, 7461–7466
42. Lee, S. Y., Jeon, H. M., Ju, M. K., Jeong, E. K., Kim, C. H., Park, H. G., *et al.* (2016) Dlx-2 and glutaminase upregulate epithelial-mesenchymal transition and glycolytic switch. *Oncotarget* **7**, 7925–7939
43. Rios Garcia, M., Steinbauer, B., Srivastava, K., Singhal, M., Mattijssen, F., Maida, A., *et al.* (2017) Acetyl-CoA carboxylase 1-dependent protein acetylation controls breast cancer metastasis and recurrence. *Cell Metab.* **26**, 842–855.e845
44. Corbet, C., Bastien, E., Santiago de Jesus, J. P., Dierge, E., Martherus, R., Vander Linden, C., *et al.* (2020) TGFβ2-induced formation of lipid droplets supports acidosis-driven EMT and the metastatic spreading of cancer cells. *Nat. Commun.* **11**, 454
45. Hua, W., Kostidis, S., Mayboroda, O., Giera, M., Hornsveld, M., and ten Dijke, P. (2021) Metabolic reprogramming of mammary epithelial cells during TGF-β-induced epithelial-to-mesenchymal transition. *Metabolites* **11**, 626
46. Nakasuka, F., Tabata, S., Sakamoto, T., Hirayama, A., Ebi, H., Yamada, T., *et al.* (2021) TGF-β-dependent reprogramming of amino acid metabolism induces epithelial–mesenchymal transition in non-small cell lung cancers. *Commun. Biol.* **4**, 782
47. Boukamp, P., Petrussevska, R. T., Breitkreutz, D., Hornung, J., Markham, A., and Fusenig, N. E. (1988) Normal keratinization in a spontaneously immortalized aneuploid human keratinocyte cell line. *J. Cell Biol.* **106**, 761–771
48. Gutierrez, E., Shin, B. S., Woolstenhulme, C. J., Kim, J. R., Saini, P., Buskirk, A. R., *et al.* (2013) eIF5A promotes translation of polyproline motifs. *Mol. Cell* **51**, 35–45

49. Schuller, A. P., Wu, C. C., Dever, T. E., Buskirk, A. R., and Green, R. (2017) eIF5A functions globally in translation elongation and termination. *Mol. Cell* **66**, 194–205.e195
50. Pegg, A. E. (2016) Functions of polyamines in mammals. *J. Biol. Chem.* **291**, 14904–14912
51. Childs, A. C., Mehta, D. J., and Gerner, E. W. (2003) Polyamine-dependent gene expression. *Cell Mol. Life Sci. (Cmls)* **60**, 1394–1406
52. Miller-Fleming, L., Olin-Sandoval, V., Campbell, K., and Ralser, M. (2015) Remaining mysteries of molecular biology: the role of polyamines in the cell. *J. Mol. Biol.* **427**, 3389–3406
53. Park, J., and Schwarzbauer, J. E. (2014) Mammary epithelial cell interactions with fibronectin stimulate epithelial-mesenchymal transition. *Oncogene* **33**, 1649–1657
54. Singh, P., Carraher, C., and Schwarzbauer, J. E. (2010) Assembly of fibronectin extracellular matrix. *Annu. Rev. Cell Dev. Biol.* **26**, 397–419
55. Jia, D., Park, J. H., Kaur, H., Jung, K. H., Yang, S., Tripathi, S., *et al.* (2021) Towards decoding the coupled decision-making of metabolism and epithelial-to-mesenchymal transition in cancer. *Br. J. Cancer* **124**, 1902–1911
56. Liu, H., and Chen, Y.-G. (2022) The interplay between TGF-β signaling and cell metabolism. *Front. Cell Dev. Biol.* **10**, 846723
57. Kang, X., Wang, J., and Li, C. (2019) Exposing the underlying relationship of cancer metastasis to metabolism and epithelial-mesenchymal transitions. *iScience* **21**, 754–772
58. Prunotto, M., Compagnone, A., Bruschi, M., Candiano, G., Colombatto, S., Bandino, A., *et al.* (2010) Endocellular polyamine availability modulates epithelial-to-mesenchymal transition and unfolded protein response in MDCK cells. *Lab. Invest.* **90**, 929–939
59. Madeo, F., Eisenberg, T., Pietrocola, F., and Kroemer, G. (2018) Spermidine in health and disease. *Science* **359**, eaan2788
60. Hofer, S. J., Simon, A. K., Bergmann, M., Eisenberg, T., Kroemer, G., and Madeo, F. (2022) Mechanisms of spermidine-induced autophagy and geroprotection. *Nat. Aging* **2**, 1112–1129
61. Arruabarrena-Aristorena, A., Zabala-Letona, A., and Carracedo, A. (2018) Oil for the cancer engine: the cross-talk between oncogenic signaling and polyamine metabolism. *Sci. Adv.* **4**, eaar2606
62. Luo, D., Lu, X., Li, H., Li, Y., Wang, Y., Jiang, S., *et al.* (2024) The spermine oxidase/spermine Axis coordinates ATG5-mediated autophagy to orchestrate renal senescence and fibrosis. *Adv. Sci. (Weinh)* **11**, e2306912
63. Blachowski, S., Motyl, T., Grzelkowska, K., Kasterka, M., Orzechowski, A., and Interewicz, B. (1994) Involvement of polyamines in epidermal growth factor (EGF), transforming growth factor (TGF)-alpha and -beta 1 action on culture of L6 and fetal bovine myoblasts. *Int. J. Biochem.* **26**, 891–897
64. Motyl, T., Kasterka, M., Grzelkowska, K., Blachowski, S., and Sysa, P. (1993) TGF-beta 1 inhibits polyamine biosynthesis in K 562 leukemic cells. *Ann. Hematol.* **67**, 285–288
65. Madeo, F., Hofer, S. J., Pendl, T., Bauer, M. A., Eisenberg, T., Carmona-Gutierrez, D., *et al.* (2020) Nutritional aspects of spermidine. *Annu. Rev. Nutr.* **40**, 135–159
66. Igarashi, K., and Kashiwagi, K. (2010) Modulation of cellular function by polyamines. *Int. J. Biochem. Cell Biol.* **42**, 39–51
67. Holbert, C. E., Dunworth, M., Foley, J. R., Dunston, T. T., Stewart, T. M., and Casero, R. A. (2020) Autophagy induction by exogenous polyamines is an artifact of bovine serum amine oxidase activity in culture serum. *J. Biol. Chem.* **295**, 9061–9068
68. Forester, C. M., Zhao, Q., Phillips, N. J., Urisman, A., Chalkley, R. J., Oses-Prieto, J. A., *et al.* (2018) Revealing nascent proteomics in signaling pathways and cell differentiation. *Proc. Natl. Acad. Sci. U. S. A.* **115**, 2353–2358
69. Sechler, J. L., Takada, Y., and Schwarzbauer, J. E. (1996) Altered rate of fibronectin matrix assembly by deletion of the first type III repeats. *J. Cell Biol.* **134**, 573–583
70. Yuan, M., Breitkopf, S. B., Yang, X., and Asara, J. M. (2012) A positive/negative ion-switching, targeted mass spectrometry-based metabolomics platform for bodily fluids, cells, and fresh and fixed tissue. *Nat. Protoc.* **7**, 872–881
71. Morgan, D. M. (1998) Determination of polyamines as their benzoylated derivatives by HPLC. *Methods Mol. Biol.* **79**, 111–118